

## Characteristics of charged particle production in relativistic heavy-ion collisions

Thomas S. Ullrich for the STAR Collaboration

Brookhaven National Laboratory, Upton New York 11973-5000, USA

**Abstract.** Inclusive spectra of charged particles at midrapidity in Au+Au collisions at  $\sqrt{s_{NN}} = 130$  GeV and 200 GeV were measured with the STAR detector at RHIC. The measured mean transverse momentum  $\langle p_T \rangle$  shows a characteristic dependence on charged particle multiplicity and beam energy in Au+Au collisions that is distinctly different from  $pp$ ,  $p\bar{p}$  and  $e^+e^-$  collisions. A  $32\% \pm 3\%$ (syst) increase in  $\langle p_T \rangle$  from pp to Au+Au collisions was observed at 200 GeV. While the charged multiplicity was found to increase by  $19\% \pm 5\%$ (syst) from  $\sqrt{s_{NN}} = 130$  GeV to 200 GeV, no significant difference in  $\langle p_T \rangle$  was found between the two energies. A comparison with model predictions is discussed.

*Keywords:* mean transverse momentum, heavy ion collisions

*PACS:* 25.75.Dw

### 1. Introduction

The systematic study of charged particle multiplicity in Au+Au collisions at center of mass energies  $\sqrt{s_{NN}} = 130$  GeV and 200 GeV was conducted by all RHIC experiments in great detail [ 1, 2, 3, 4, 5, 6]. These studies were accompanied by intensive theoretical work successfully connecting the produced particle densities with the initial conditions in these collisions. Essentially all models that attempt to describe the evolution of matter produced in relativistic heavy-ion collisions predict a strong correlation between the average transverse momentum and the multiplicity of the event, typically  $\langle p_T \rangle^2 \propto dN_{ch}/d\eta$ . This simply reflects the basic thermodynamic concept inherent to the models: large  $N_{ch}$  means large entropy, large entropy means higher temperature  $T$ , which, following the general concepts of Landau's hydrodynamical model, implies an increase in  $\langle p_T \rangle$ . The use of thermodynamics in this argument does not, of course, preclude a dynamical description in terms of (non-)perturbative Quantum Chromodynamics (QCD). It simply takes advantage of the fact that if the actual physical states of the system are close to a canoni-

cal distribution, thermodynamics is an ideal tool to analyze the measurements and relate them to bulk properties of hot matter.

One prominent class of models that allows a direct coupling of global observables with the initial conditions of the collision are those based on the concept of gluon saturation. In these models particle production is related to the initial gluon distribution. A semi-classic calculation can be carried out due to the high gluon density, a saturation phenomenon also known as the Color Glass Condensate [ 7, 8]. The only scale that controls the gluon distribution at a given Bjorken  $x$  is the saturation momentum scale  $Q_s$ . If the gluons realize themselves directly to hadrons, the transverse momentum of the hadrons will be directly related to the saturation scale  $Q_s$  as well as the multiplicity of the particle production [ 8, 9]. In fact, this assumption was used in some predictions that successfully predicted the particle multiplicity along with their centrality and pseudorapidity dependence [ 8].

So far, however, only few studies were undertaken to verify if these models are also able to describe the characteristics of  $\langle p_T \rangle$  at RHIC. In this article we present results on the characteristics of (i) the charged particle densities **and** (ii) of  $\langle p_T \rangle$  using data recorded by the STAR experiment.

## 2. Inclusive charged hadron spectra

The data reported here were taken with the Solenoidal Tracker at RHIC (STAR) [ 10]. The main tracking device in STAR is a large Time Projection Chamber (TPC) which provides momentum information and particle identification for charged particles by measuring their ionization energy loss. A Central Trigger Barrel (CTB) constructed of scintillator paddles surrounding the TPC and two Zero Degree Calorimeters (ZDC) were used for triggering. Data were taken for Au+Au collisions at  $\sqrt{s_{NN}}=130$  GeV in the summer of 2000 (run I) and  $\sqrt{s_{NN}}=200$  GeV in the fall of 2001 (run II). The field setting for run I was at 0.25 T while at run II it was at the nominal field setting of 0.5 T. The increased field resulted in a factor of three improvement in momentum resolution. In both runs a minimum bias trigger was defined by using coincidences between the two ZDCs located  $\pm 18$  meters away from the interaction point. For details see Ref. [ 11].

To measure the differential invariant cross-section of the produced charged particle for different centralities tracks with transverse momenta between 0.2 and 2.0 GeV/ $c$  were selected. The reconstruction efficiency was determined by embedding simulated tracks into real events at the raw data level, reconstructing the full events, and comparing the simulated input to the reconstructed output. Charged hadrons ( $h^+ + h^-$ )/2 were approximated by the summed yields of  $\pi^\pm$ ,  $K^\pm$ ,  $p$  and  $\bar{p}$ . The efficiencies for the identified particles are between 70% and 80% for central events at  $p_T > 0.5$  GeV/ $c$ . At lower  $p_T$  (0.2 to 0.5 GeV/ $c$ ), the efficiency for pion is about 70% and the efficiencies of kaon and antiproton are from 30% to about 70% due to energy loss, absorption and decay in the detector. The final efficiency of the charged particle spectrum is the weighted efficiency of all  $\pi^\pm$ ,  $K^\pm$  and  $p^\pm$  according

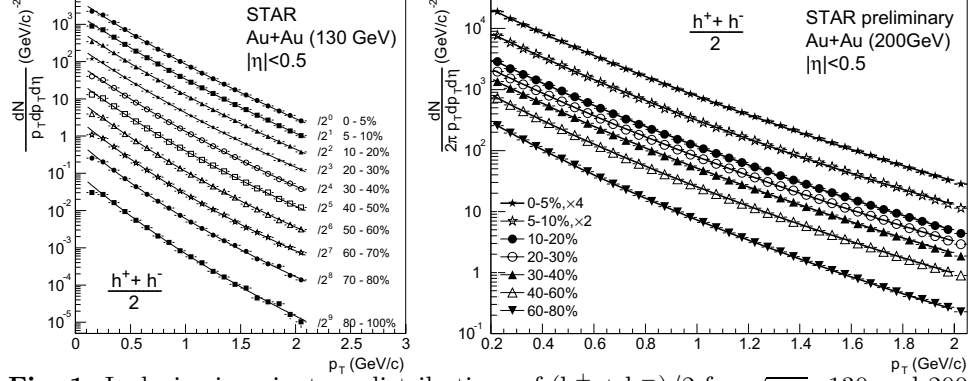


**Fig. 1.** Inclusive invariant  $p_T$  distributions of  $(h^+ + h^-)/2$  for  $\sqrt{s_{\text{NN}}}=130$  and 200 GeV Au+Au collisions. The lines are power law fits to the data (see text).

to their yield ratios measured at  $\sqrt{s_{\text{NN}}} = 130$  GeV and the proper Jacobian factor  $\partial y / \partial \eta(p_T, \eta)$ . It is almost identical to that of the pions for all  $p_T$ .

Background particles mis-identified as primary particles originate from various sources. The dominant ones are: hadrons from weak decays of  $K_S^0$ ,  $\Lambda$  and  $\bar{\Lambda}$ , weak decays of primary charged particles, and hadrons from secondary interactions in the detectors. The background corrections for the former were calculated by using measured yields and spectra. The later two are important only at low  $p_T$  and we used HIJING with a detailed detector simulation to reproduce the background spectra for each centrality.

Figure 1 shows the fully corrected inclusive  $p_T$  distributions of primary charged particles for  $\sqrt{s_{\text{NN}}}=130$  and 200 GeV Au+Au collisions for 10 and 7 centrality bins, respectively. The spectra were fit with a power law function of the form  $A(1 + p_T/p_0)^n$ . The average momentum is defined as  $\langle p_T \rangle = 2 p_0 / (n - 3)$ . To extract the  $\langle p_T \rangle$  we substitute  $p_0$  by  $\langle p_T \rangle (n - 3) / 2$  and fit the spectrum with  $\langle p_T \rangle$  and  $n$  as a free parameters. The difference between the integral of the fit function and the sum of the data points in the fiducial kinematic range is less than 1%. The extrapolation to the total  $p_T$  is 21-26% from central to peripheral centrality. The systematical uncertainty of  $\langle p_T \rangle$  was estimated to 2%. The function, fit in the range of 0.2 GeV/c to 2.0 GeV/c, was then extrapolated to the full transverse momentum range to get the total  $N_{\text{ch}}$ . The systematical uncertainty on  $N_{\text{ch}}$  is 7%.

For the 5% most central collisions. The charged hadron multiplicity at  $\sqrt{s_{\text{NN}}}=200$  GeV (130 GeV) is  $dN_{\text{ch}}/d\eta|_{|\eta|<0.5} = 690 \pm 55(\text{syst})$  ( $579 \pm 60(\text{syst})$ ) and the mean transverse momentum  $\langle p_T \rangle$  is  $0.517 \pm 0.012 \text{ GeV/c}$  ( $0.519 \pm 0.01 \text{ GeV/c}$ ). For  $\sqrt{s_{\text{NN}}}=200$  GeV the multiplicity per participant pair increases by 38% relative to  $p\bar{p}$  and 52% compared to nuclear collisions at  $\sqrt{s_{\text{NN}}}=17$  GeV. The  $\langle p_T \rangle$  increases by 32% and 20% respectively from 0.392 GeV/c in  $p\bar{p}$  collisions and  $\simeq 0.429$  GeV/c in Pb+Pb collisions at SPS [ 11, 12].

### 3. Centrality dependence of charged particle densities

The RHIC experiments all have different methods of determining centrality. In general, all measure some final state variable (or combination of these variables) that can be related to fractions of the total measured hadronic cross-section. These centrality bins are then mapped to variables that allow for direct comparison between experiments. The primary variables that are used for comparison are *(i)* the number of participating nucleons in the collision  $N_{\text{part}}$  and *(ii)* the number of binary collisions  $N_{\text{bin}}$ , which are determined via the application of the Glauber model phenomenology. The basic concept of the Glauber model is to treat a Au+Au collision as a superposition of many independent nucleon-nucleon (N+N) collisions. Thus, the only parameters that the model depends on are a nuclear density profile (Woods-Saxon) and the non-diffractive inelastic N+N cross-section. The former is well measured in e+Au scattering experiments. The latter is well established by many previous experiments. With this, it is possible to determine both the total number of independent N+N collisions ( $N_{\text{bin}}$ ) and the total number of nucleons that participate in the collisions ( $N_{\text{part}}$ ) as a function of impact parameter ( $b$ ). There are two separate implementations of the Glauber model: Optical and Monte Carlo. In the optical formalism  $N_{\text{bin}}$  and  $N_{\text{part}}$  are directly determined by an analytic integration of overlapping Woods-Saxon distributions. In the M.C. method an arbitrary number of events are simulated using a computer program and the resulting distributions of  $N_{\text{bin}}$  and  $N_{\text{part}}$  are determined. Once the distributions  $d\sigma/dN_{\text{part}}$  and  $d\sigma/dN_{\text{bin}}$  are determined, these histograms are binned according to fractions of the total cross-section. This determines the mean values of  $N_{\text{bin}}$  and  $N_{\text{part}}$  for each centrality class. In this context it should be noted that in the M.C. approach one requires that all nucleons in either nucleus be separated by a distance  $d \geq d_{\text{min}}$  where  $d_{\text{min}} = 0.4$  fm is characteristic of the length of the repulsive nucleon-nucleon force. Consequently the total Au+Au cross section predicted by the Monte Carlo approach depends strongly on  $d_{\text{min}}$ . A value of  $d_{\text{min}} = 0.4$  fm yields a total cross-section of 7.2 barns, while  $d_{\text{min}} = 0$  fm yields 6.8 barns.

While at SPS energies both approaches yielded consistent answers, at RHIC energies, the optical approach may yield systematically smaller values of the total Au+Au cross-section. Therefore, any results reported in terms of Glauber quantities must be carefully interpreted based upon specifics of the Glauber calculations.

In the case of STAR the centrality was determined by the multiplicity of all charged particles within  $|\eta| < 0.5$  and then expressed in terms of the fractional total hadronic cross section. The measured data, i.e. the  $dN/dN_{\text{ch}}$  distributions, are then mapped to the corresponding distribution obtained from Glauber calculations as described above, thus relating  $N_{\text{part}}$  and  $N_{\text{bin}}$  to the measured distributions.

Figure 2 shows the extracted yields as the pseudo-rapidity density per participant pair  $2/N_{\text{part}} dN/d\eta$  versus the number of participants  $N_{\text{part}}$  for Au+Au collisions at  $\sqrt{s_{\text{NN}}} = 130$  GeV, where for the left plot we used a Monte Carlo Glauber calculation to derive  $N_{\text{part}}$  while for the right plot we used an optical Glauber model.

The parameterization of pseudo-rapidity density of the EKRT model [13], a

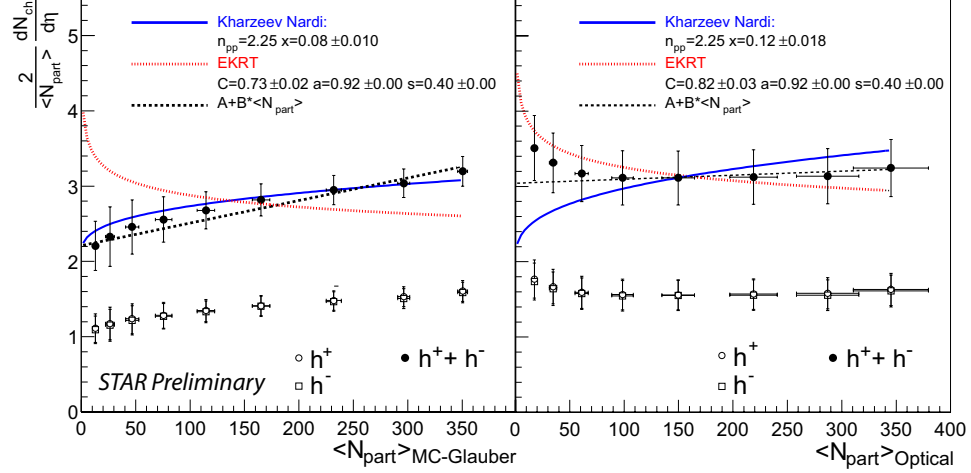


**Fig. 2.** Rapidity density per participant nucleon pair  $2/\langle N_{\text{part}} \rangle dN/d\eta$  versus number of participants  $\langle N_{\text{part}} \rangle$ . On the left plot  $N_{\text{part}}$  was calculated using a MC Glauber approach while on the right plot an optical Glauber model was used.

model based on the assumption of final state gluon saturation, fails to describe the data when using the Monte Carlo Glauber calculations, but agrees nicely with when using the optical Glauber calculation. Both, our data and the EKRT parameterization do not approach the charged particle pseudo-rapidity density  $n_{pp} = 2.25$  (measured from non-single diffractive  $p\bar{p}$  interactions and parameterized as  $n_{pp} = 2.5 \pm 1.0 - (0.25 \pm 0.19) \ln(s) + (0.023 \pm 0.008) \ln^2(s)$  [ 14]) in the limit of  $N_{\text{part}}=2$ . One might argue that the model breaks down for very peripheral collisions. The centrality dependence from mid-central to central collisions is in fact too weak to rule out the EKRT model.

Comparing the two-component model described in Ref. [ 15] with our data shows the exact opposite behavior. Fitting the proposed function to our data we find agreement between the fit and our measurement only when using the Monte Carlo Glauber calculation (left plot in Fig. 2). Here, we evaluate the fraction of hard collisions  $x_{\text{hard}}$  as  $0.08 \pm 0.01$  for our most central events. The fraction of produced particles originating from hard collisions is then calculated as  $F_{\text{hard}} = x n_{pp} N_{\text{bin}} / (dN_{\text{ch}}/d\eta) = 0.36 \pm 0.2$ . Both values  $x_{\text{hard}}$  and  $F_{\text{hard}}$  agree nicely with the numbers quoted by Ref. [ 4] and [ 15].

It should be noted that in general the M.C. Glauber method is considered to be more accurate than the calculations in the optical limit. Nevertheless, in both approaches the systematic uncertainties in the calculation of  $N_{\text{part}}$  are considerable large for very peripheral collisions, the region where the differences between the various models become more apparent. For the centrality fraction of 70-80% the uncertainty on  $N_{\text{part}}$  already reaches 30%.

#### 4. Characteristics of $\langle p_T \rangle$ in heavy-ion collisions

Using the spectra from Fig. 1 and the power law fits described above we now turn to the centrality dependence of  $\langle p_T \rangle$ .

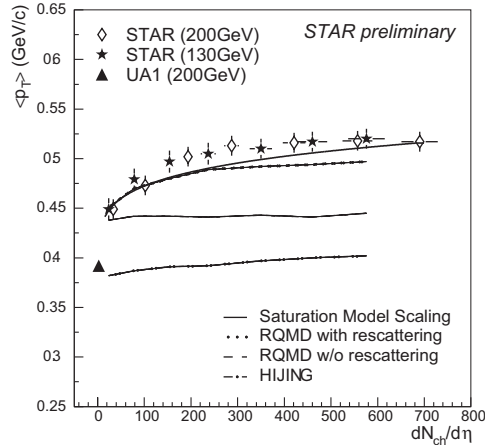
Figure 3 shows the  $\langle p_T \rangle$  as a function of charge multiplicity for both energies. The open symbols are from 200 GeV data and the solid stars are measurements from 130 GeV data. The solid triangle depicts the UA1 measurement [16]. We also show the calculation from Eq. 1 discussed in more details below. The simulations from RQMD with and without rescattering are shown as dotted and dashed lines, respectively. The dot-dashed line depicts the simulation from HIJING with default settings. The  $\langle p_T \rangle$  increases as function of centrality from peripheral to semi-central collisions and seems to reach a plateau for central collisions.

Figure 4 has two panels. The solid triangles in the top panel depict the inclusive charged particle ratios between 130 GeV and 200 GeV as a function of number of participants (neglecting the small difference of  $N_{\text{part}}$  between these two beam energies). The open diamonds are measurements from the PHOBOS Collaboration [3]. For central collisions the charged particle multiplicity increases from 130 GeV to 200 GeV by 19%. This result is comparable with the results from other RHIC experiments [3]. However, the systematical uncertainty at peripheral collisions is too large to be conclusive as shown in the top panel. Surprisingly, one finds no increase of  $\langle p_T \rangle$  within the current systematic errors for any centrality bin as depicted in the bottom panel.

Figure 5 shows  $\langle p_T \rangle$  of negatively charged particles  $h^-$  from NA49 and charged particles  $(h^+ + h^-)/2$  from various other experiments as function of  $\sqrt{s_{\text{NN}}}$  for  $pp$ ,  $\bar{p}p$  and central AA collisions. The dotted line is a parametrization of the measured  $\langle p_T \rangle$  in  $pp$  collisions [16]. For the  $e^+e^-$  data, the dot-dashed line is a prediction from JETSET [17]. The fact that the  $\langle p_T \rangle$  from AA collisions is distinctly different from both  $pp$  and  $e^+e^-$  indicates that AA collisions are not simple superpositions of the elementary collisions.

As already discussed in the introduction, saturation [9] and hydrodynamical [18] models predict some scaling behavior of  $\langle p_T \rangle^2 \sim (\frac{dN}{d\eta})_{AA} / \pi R^2$ .

In order to get a quantitative analysis on the dependence between  $\langle p_T \rangle$  and



**Fig. 3.**  $\langle p_T \rangle$  as a function of  $N_{\text{ch}}$  at  $\sqrt{s_{\text{NN}}} = 130$  GeV and 200 GeV. The solid line is a prediction assuming scaling of  $\langle p_T \rangle$  with  $N_{\text{ch}}$  as described in the text. Also shown are the simulations from RQMD with and without rescattering and HIJING 1.35. All model curves are for  $\sqrt{s_{\text{NN}}} = 130$  GeV only.

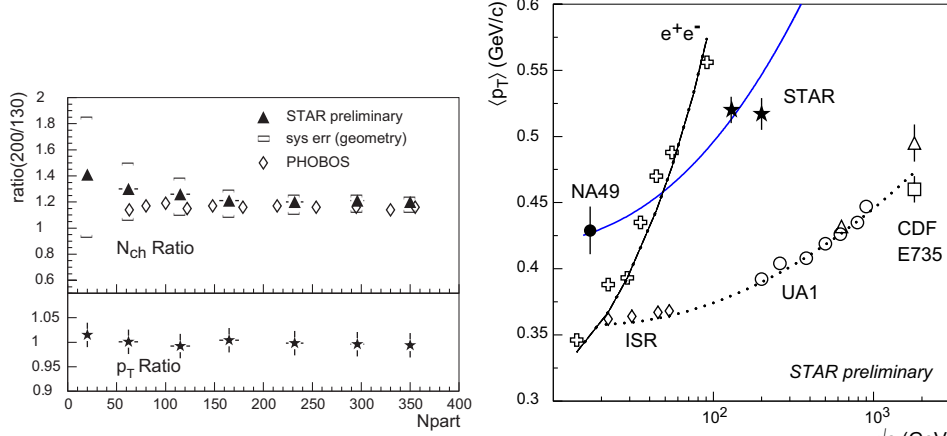


**Fig. 4.** Ratios of  $N_{ch}$  and  $\langle p_T \rangle$  between  $\sqrt{s_{NN}}$  of 200 GeV and 130 GeV Au+Au function of  $\sqrt{s_{NN}}$  for  $pp$   $\bar{p}p$  and central AA collisions. The open symbols are ratios collisions. The  $\langle p_T \rangle$  from  $e^+e^-$  was calculated along the jet thrust axis.

multiplicity, we require that the scaling dependence is linear and it should also satisfy the  $pp$  results. Thereby, there is only one free parameter as shown in Eq. 1:

$$\langle p_T \rangle_{AA} = a + \sqrt{\frac{s_{AA}}{s_{pp}}} (\langle p_T \rangle_{pp} - a); \quad (1)$$

where  $s_{AA} = (dN/d\eta)_{AA}/\pi R^2$  and  $s_{pp} = (dN/d\eta)_{pp}/\pi r_0^2$  are the multiplicity densities per unit pseudorapidity per unit transverse area in AA and pp collisions ( $R = r_0 A^{1/3}$ ) and  $a = 0.3$  GeV/c is a constant chosen to describe the AA data. For non-central collisions, the calculation of the transverse area is not straight forward. We take the centrality dependence parametrization of  $s_{AA}$  from Ref. [9]. The solid curves in Fig. 3 and Fig. 5 show the energy dependence and centrality dependence of  $\langle p_T \rangle$  from Eq. 1. The curves describe the data well from SPS to RHIC at 130 GeV. However, the data show that the increase in  $\langle p_T \rangle$  from  $\sqrt{s_{NN}} = 130$  to 200 GeV is not as strong as the thick-line indicates which may invalidate the scaling law from the saturation model [9]. On the other hand, the energy dependence might indicate the importance of early thermalization in the partonic stage, as proposed in ref [19]. Such initial partonic activity is consistent with the early development of flow as indicated from  $\langle v_2 \rangle$  measurements at RHIC [20]. It will be interesting to see if the description holds with an energy scan of lower beam energies at RHIC.

## 5. Summary

In summary, STAR has measured charged particle multiplicities and transverse momentum spectra at mid rapidity in Au+Au collisions at  $\sqrt{s_{NN}} = 130$  GeV and 200 GeV. Their centrality and beam energy dependences are distinctly different

from elementary collisions ( $e^+e^-$ ,  $pp$  and  $\bar{p}p$ ). The saturation model with direct hadron production from gluons seems unable to explain the lack of increase in  $\langle p_T \rangle$  from 130 GeV to 200 GeV. However, the saturation model with thermalization [19] might be consistent with our result. Further measurements with various beam energies and beam species such as d+Au may be able to further distinguish different production mechanisms.

## Acknowledgment

The author thanks F. Laue, M. Miller, and Z. Xu for valuable contributions for this article.

## References

1. T.S. Ullrich, Nucl. Phys. A715, 399c-411c (2003).
2. B.B. Back *et al.*, Phys. Rev. C65, 31901R (2002).
3. B.B. Back *et al.*, Phys. Rev. Lett. 88, 22302 (2002).
4. B.B. Back *et al.*, Phys. Rev. C65, 061901R (2002).
5. K. Adcox *et al.*, Phys. Rev. Lett. 86, 3500 (2001).
6. I.G. Bearden *et al.*, Phys. Lett. B523, 227 (2001).
7. L. McLerran, Lect. Notes Phys. 583, 291 (2002); hep-ph/0104285.
8. D. Kharzeev and E. Levin, Phys. Lett. B523, 79-87 (2001).
9. L. McLerran *et al.*, Phys. Lett. B514, 29 (2001); J. Schaffner-Bielich *et al.*, nucl-th/0202054.
10. C. Adler *et al.*, Nucl. Instr. Meth. A499, no. 2+3 (2003).
11. C. Adler *et al.*, Phys. Rev. Lett. 87, 112303 (2001).
12. H. Appelshäuser *et al.*, Phys. Rev. Lett. 82, 2471 (1999).
13. K. Eskola *et al.*, Nucl. Phys. B570, 379 (2000); hep-ph/9909456.
14. F. Abe *et al.*, Phys. Rev. D41, 2330 (1990).
15. D. Kharzeev and M. Nardi, Phys. Lett. B507, 121-128 (2001).
16. C. Albajar *et al.*, Nucl. Phys. B335, 261 (1990).
17. R. Akers *et al.*, Phys. Lett. B320, 417(1994).
18. D. K. Srivastava, Phys. Rev. C64, 06490 (2001).
19. A. Mueller *et al.*, Nucl. Phys. A715, 20c (2003); R. Baier *et al.*, Phys. Lett. B539, 46 (2002).
20. K.H. Ackermann *et al.*, Phys. Rev. Lett. 86, 402(2001); C. Adler *et al.*, Phys. Rev. Lett. 87, 112301 (2001);